Room temperature manipulation of long lifetime spins in metallic-like carbon nanospheres

Bálint Náfrádi[1], Mohammad Choucair[2], Klaus-Peter Dinse[3] & László Forró[1]

The time-window for processing electron spin information (spintronics) in solid-state quantum electronic devices is determined by the spin–lattice and spin–spin relaxation times of electrons. Minimizing the effects of spin–orbit coupling and the local magnetic contributions of neighbouring atoms on spin–lattice and spin–spin relaxation times at room temperature remain substantial challenges to practical spintronics. Here we report conduction electron spin–lattice and spin–spin relaxation times of 175 ns at 300 K in 37 ± 7 nm carbon spheres, which is remarkably long for any conducting solid-state material of comparable size. Following the observation of spin polarization by electron spin resonance, we control the quantum state of the electron spin by applying short bursts of an oscillating magnetic field and observe coherent oscillations of the spin state. These results demonstrate the feasibility of operating electron spins in conducting carbon nanospheres as quantum bits at room temperature.

[1] Laboratory of Physics of Complex Matter (LPMC), Ecole Polytechnique Fédérale de Lausanne, 1015 Lausanne, Switzerland. [2] School of Chemistry, University of Sydney, Sydney, New South Wales 2006, Australia. [3] Institut für Experimentalphysik, Freie Universität Berlin, Arnimallee 14, 14195 Berlin, Germany. Correspondence and requests for materials should be addressed to B.N. (email: balint.nafradi@epfl.ch) or to M.C. (email: mohammad.choucair@sydney.edu.au).

Electron spin states are an attractive realization of a quantum bit (qubit) as they can undergo a transition between the spin-up and spin-down quantum states[1]. The most commonly used technique for manipulating electron spin is electron spin resonance (ESR)[2]. ESR is the physical process, whereby electron spins are polarized in an external magnetic field $\mathbf{B}_0$ and rotated by an oscillating magnetic field $\mathbf{B}_1$ (perpendicularly to $\mathbf{B}_0$, of frequency f), which is resonant with the spin precession frequency in an external magnetic field $f = g\mu_B B_0/h$ (μ_B is the Bohr magneton and g the electron spin g-factor, h is the Planck's constant). ESR is result of the coherence of the precession of electrons over the spin–lattice and spin–spin relaxation times, T_1 and T_2, respectively[3]. T_1 is characterized by a number of spin–lattice relaxation process that depend on the spin–orbit coupling to connect the spin of an electron with the lattice vibrational spectrum of the solid. The second important relaxation time T_2 is set by the probability of spin–spin relaxation. T_2 is concerned with the local magnetic field contribution by one magnetic atom on others and represents the phase coherence of a set of spins. The dominant relaxation time is the shorter of T_1 and T_2. In magnetically homogenous itinerant systems (for example, metals), the condition $T_1 = T_2$ is often met and represents the longest period of time that in-phase precessing electron spins and magnetization can propagate as a uniform mode[4].

Electron spin states therefore need to be robust against decoherence. The feasibility of applications involving classical or quantum information processing is hence critically dependent on T_1 and T_2 relaxation times[5–12]. The prerequisite for T_1 and T_2 relaxation times is ~ 100 ns, as this is the state of the art lower-bound for signal processing times in quantum electronic devices[13,14].

Advances in the fields of inorganic[15,16] and molecular[17,18] quantum dots have made the electron spin system promising for practical application in spintronic and quantum information processing. Current research activities on spin-based qubits are divided into two distinct research directions with limited overlap and are based on the materials employed: inorganic materials, usually semiconducting structures forming quantum dots, and carbon-based molecules. The qubits utilized in these materials are also different: inorganic materials containing localized spins of doped ions or conduction electron spin confined on quantum dots, whereas organic materials utilize localized paramagnetic spins confined on molecules.

Due to the radical differences in the materials and the electron systems employed for spin qubit manipulation, the major challenges to realising devices are also distinct. For solid-state inorganic materials the strong spin–orbit interaction enforced by heavy nuclei in materials like semiconductors[10,11,19] and metals[12,20,21] strongly requires the pursuit of structural perfection and spin manipulation at low temperatures (40 mK to 100 K). This has resulted in well-defined materials that currently set the benchmark for long T_1 relaxation times exceeding seconds[9]. Unfortunately, at room temperatures a number of intrinsic spin–lattice relaxation processes and phonon modes induce spin decoherence and diminish T_1 and T_2 (ref. 22). Consequently, for metal nanoparticles[21] T_1 and T_2 shortens to 10–40 ps and for bulk semiconductors[23,24] to 1–4 ns.

Molecular qubits can be produced on an industrial scale and are readily processed[18]. These spin-bearing organic molecules often have low spin–orbit coupling, possess many non-degenerate spin transitions, and can be chemically modified. These attributes have led to the potential of molecular compounds for both spintronics and quantum information processing. However, the dipole–dipole interactions between molecules and the hyperfine interaction of the molecule requires diluting the spin containing molecules and isotope engineering of the host system to reduce magnetic inhomogeneity. It also needs low temperatures (<100 K) for spin manipulation to dampen molecular vibrations that cause spin decoherence.

Attempts to combine the advantages of inorganic and molecular qubit materials have led to electronically insulating systems like nitrogen-vacancy (N-V) centre nanodiamonds[25] and N@C_{60} (refs 14,26). Long microsecond T_1 and T_2 of localized electrons in these materials can be achieved and manipulated at ambient conditions. Magnetic inhomogeneity in these materials is accounted for by isotopic engineering constituent ^{13}C and $^{14,15}N$ nuclei, however, the localized electron spins themselves generate fluctuating magnetic fields, posing limitations on the qubit density. This limitation is specific to localized electron systems and it is absent for conduction electrons where the motional narrowing process negates this effect[27].

Carbon nanotube-based quantum dots have been prepared with an electron spin dephasing time of ~ 3 ns at millikelvin temperature[28]. The shortening of T_2 in these carbon nanotubes is attributed to an increase in the spin–orbit coupling induced by the high curvature of the carbon sheets[29]. Graphene on the other hand is comprised entirely from a single-atom thick crystalline layer of carbon, is flat (or at best not curved), and conducting[30,31]. Experiments on single- and few-layer graphene have demonstrated $T_1 = T_2$ of 1–4 ns at room temperature[32]. However, this value is still far below expectations for practical use and possibly limited by physisorption and chemisorption of molecular oxygen or other species onto the unprotected carbon surface[33]. Non-carbon-based materials have also been developed, including heterometallic molecular nanomagnets comprising of isotopically engineered and diamagnetically diluted Cr_7M (M = Ni, Mn, Zn) that demonstrate the prerequisite for quantum processing applications at low temperature (5 K) (ref. 34).

These possible solutions demonstrate that there are clear and established trade-offs to be considered regarding the feasibility of applying a qubit material system: a conducting material of light atomic weight constituents that meets the prerequisite T_1 and T_2 at room temperature would permit real spintronics and quantum processing applications. Such a material would combine the best aspects of both inorganic and molecular spin qubit schemes.

Here we report the observation of $T_1 = T_2 = 175$ ns at room temperature (300 K) in conducting metallic-like carbon nano-spheres via ESR. Furthermore, we could coherently control the quantum state of the electron spin confined on the carbon nanospheres at 300 K. This remarkable result can be put in context by comparing it with other promising systems, which could carry the quantum bit: N@C_{60}, N-V centre in nanodia-mond or P-doped Si (Fig. 1). In the carbon nanospheres, the electron spins are highly delocalized and polarizable (Pauli-paramagnetic) over the volume of the nanosphere, rather than highly confined to a small path on the order of the electron orbit, as would be the case for a localized electron system. This has the advantages that there is no need for isotopic engineering of the carbon nuclei to suppress magnetic inhomogeneity, and an absence of fluctuations in local magnetic fields of localized spins. The material thus allows a higher density packing of qubits to be, in principle, achieved over other promising qubits.

Results

The structural and chemical properties of the carbon nanospheres are inherently key to the observation of the long $T_1 = T_2$. Transmission electron microscopy (TEM) images show the extensive formation of spherical carbon spanning micron scales (Fig. 2a and Supplementary Fig. 1). The as-prepared carbon nanospheres are a conglomeration of spherical bodies and after
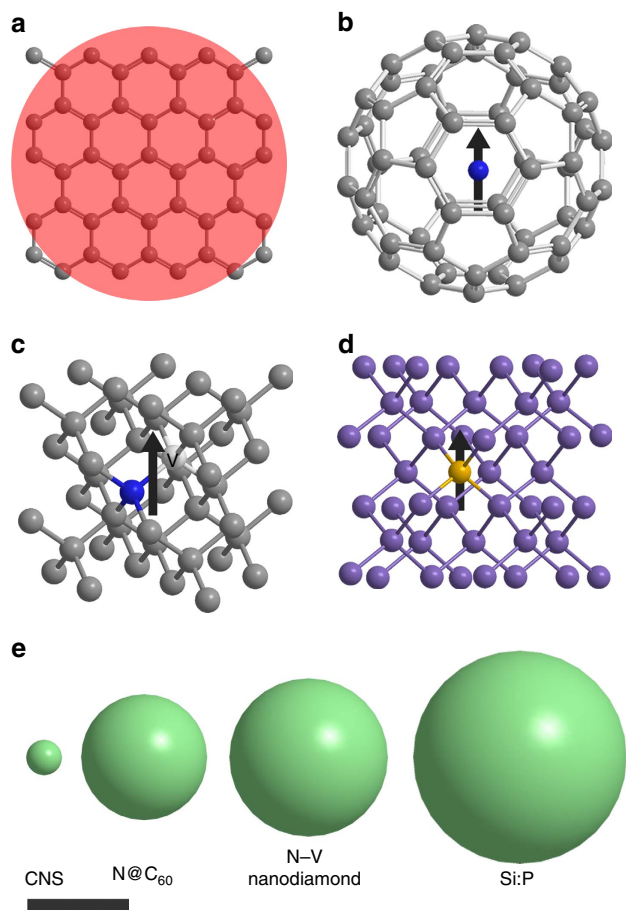
Figure 1 | Comparison of itinerant and localized electron-based qubits.
(**a**) Itinerant spin system of carbon nanospheres (CNS), and localized spin systems of (**b**) N@C_{60}, (**c**) N-V nanodiamond and (**d**) Si:P. The spin information in the CNS is encoded by a delocalized electron spin that spreads over the entire 35-nm diameter (shaded area), making the system more robust against external magnetic field fluctuations and hyperfine interactions enforced by nuclear spins. Consequently, high qubit density can be achieved without enhanced decoherence. (**e**) The sphere diameters comparing the required volume for different types of qubits[14,25,50] with scale bar, 100 nm.

X-ray photoelectron spectroscopy (XPS), thermogravimetric analysis (TGA), and Raman experiments were also performed and are found in Supplementary Figs 4–9 and Supplementary Notes 1–3. XPS indicated that the chemical structure is predominately conducting graphitic carbon (90.2 wt%) containing surface bound oxygen (9.8 wt%), and there was no inclusion of metals and other heavy atoms. TGA experiments confirmed the carbon nanosphere material did not contain residual precursor polyaromatic hydrocarbons and remained chemically and thermally stable even up to temperatures of 883 K. Valence band XPS revealed the presence of non-bonding π and σ orbitals as a result of fragmented sheets that contained carbon arranged in a distorted hexagonal network.

The carbon nanospheres are easily synthesized[36] and readily processable (Fig. 3), yielding a homogenous material that is structurally highly non-crystalline (Fig. 2). Thus the carbon nanospheres can be reliably employed for spintronics applications with minimal processing and without the need for fabricating a well-defined crystal structure to achieve long T_1 and T_2. Furthermore, in a conducting carbon nanosphere qubit system, the rich chemistry of carbon can, in future experiments, allow for a myriad of non-covalent and covalent interactions to connect the nanospheres to conducting electronic device surfaces[37,38]. Finally, the carbon nanospheres are of a size that can be isolated on a surface from the 'top-down' using micromanipulator probe tips (Fig. 3d), and this in future experiments can allow for building qubit ensembles[39].

Here we develop in more detail our key observations obtained by ESR. At 300 K and at 9.4 GHz frequency the continuous-wave ESR line width (peak-to-peak) is $\Delta H = 0.056$ mT (inset Fig. 4a and Supplementary Fig. 10) and the g-value is 2.00225 (inset Fig. 4b). This is a remarkably narrow conduction-electron spin ESR line testifying the long spin-relaxation times. The observed spectra had, to a high precision, homogeneously broadened Lorentzian line shapes and the deviation from the Lorentzian line shape in the entire spectra was <5%, (see Supplementary Fig. 10 as an example), which reveals the itinerant nature of the spins. The observed linewidth determined by continuous-wave ESR is identical within the experimental error with the T_2-derived Lorentzian width. Note that the size distribution of the carbon nanospheres has a negligible effect on the linewidth at 9.4 GHz because of the motional narrowing of conduction electrons (Supplementary Fig. 11). The hyperfine ESR lines of ^{13}C were also absent (which are readily observable for localized spins[14,25,26]) due to motional narrowing of conduction electrons[27]. The g-factor is characteristic to conduction electrons of carbon, and it does not originate from metallic inclusions (in agreement with our chemical analysis) or from localized paramagnetic 'dangling' bonds of carbon (commonly with $g = 2.00282$) (ref. 40).

In addition to the continuous-wave ESR experiment, where detection and spin rotation occur at the same time, we extended our experiments to probe the spin relaxation dynamics of T_1 and T_2 independently using pulsed ESR (Fig. 4a). At 9.5 GHz frequency and 300 K, with good approximation we found that the intrinsic $T_1 = T_2 = 175$ ns. Pulsed ESR therefore simultaneously validated our continuous-wave ESR results and verified that the line-shape obtained by continuous-wave ESR was indeed homogenous as expected for itinerant electrons.

The temperature-dependent properties of the ESR spectra (Fig. 4 and see also Supplementary Fig. 12) support that conduction electrons are confined within the carbon nanospheres. The g-factor was temperature independent (Fig. 4d), which is in good agreement with general observations in metals with weak spin–orbit coupling and in graphitic nanoparticles[41]. The resulting spin susceptibility is temperature dependent, following a Curie–Weiss dependence, as one may expect for nanoparticles of metals (Fig. 4b)[21,42].
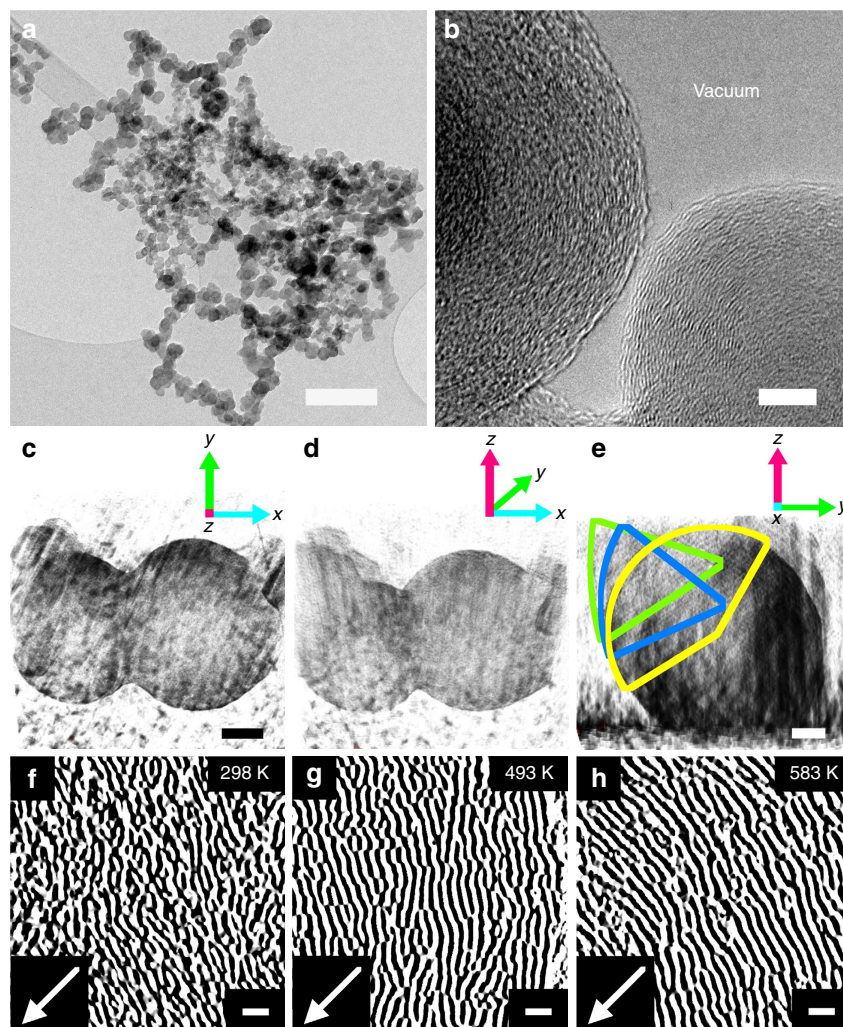
sonication in suspension they could appear as individual particles (Fig. 2b). In comparison with other nanoparticle quantum dots used as qubits, for example, Mn-doped PbS (ref. 35), the carbon nanospheres are relatively uniform with a size distribution of 37 ± 7 nm estimated from TEM images (Supplementary Fig. 2).

By means of TEM tomography, a number of carbon nanospheres are also observed to have an asymmetric shape, which also results from the formation of joint graphitic layers of contacting particles (Fig. 2c–e), with the accretion of layers between nanospheres generally forming within a region of ca. 5 nm of the outer layers (Supplementary Fig. 3). High-resolution TEM revealed the short graphitic fragments that comprise the carbon nanospheres are graphitic fragments that follow the curvature of a sphere, creating many open edges (Fig. 2f–h). The individual graphitic fragments in the carbon nanospheres are not curved and do not resemble the curvature in nanotubes or fullerenes. Rather, the fragments exhibit an intricate array of interplanar bonding all the way to the centre of the nanosphere even when heated to temperatures of 583 K. The carbon nanospheres are not hollow and show a continuation of the closed cage structure towards the centre.

Figure 2 | Carbon nanosphere structure and size. (**a**) TEM image of carbon nanospheres on a carbon support. (**b**) High-resolution TEM of discrete carbon nanospheres. (**c–e**) TEM three-dimensional tomography reconstruction of the carbon nanospheres. The particles are spherical and also distort slightly to an ellipsoidal shape, with coalescence. Spheres appear transparent due to the high image contrast with the sputtered gold substrate, small sphere size and extremely thin sphere layers. (**f–h**) *In situ* variable temperature high-resolution TEM images of the non-crystalline carbon nanosphere structure within regions of various spheres. The spheres remain non-crystalline upon heating to 583 K. A high contrast is applied to the images to allow the graphite planes to be distinguished with a black outline. Arrows indicate direction towards the centre of the sphere. Scale bars, 200 nm (**a**), 5 nm (**b**), 10 nm (**c**), were omitted for clarity (**d**), 5 nm (**e**), 1 nm (**f–h**).

Multi-frequency ESR in the 4–420 GHz frequency and 2–300 K temperature range also confirmed that conduction electrons are confined within the carbon nanoparticles (Fig. 4 and Supplementary Fig. 12)[43,44]. The ESR linewidth revealed a linear increase with increasing magnetic field at 300 K (Fig. 4c and see also Supplementary Fig. 12). Note that in the case of bulk metals, ΔH is solely determined by spin–orbit coupling thus it is independent of the magnetic field[21,45]. However, the behaviour observed when the carbon nanospheres experience a variation in external magnetic field is characteristic to conduction electrons enclosed in nanoparticles where T_1 and T_2 are determined by both the spin–orbit interaction and electron confinement[21]. This broadening of ΔH for itinerant electrons confined on small particles follows[46]:

$$\Delta H = E_Z/(\delta\gamma_e T_2) \tag{1}$$

where $E_Z = h\nu_Z$ is the Zeeman energy, δ is the average electronic energy level spacing and γ_e is the electron gyromagnetic ratio[46]. Using the measured $T_1 = T_2 = 175$ ns, we can extract a $\delta = 1$ meV for the average electronic energy level spacing (linear line of best

fit in Fig. 4c). From this value one can calculate back the size of the carbon spheres by following Kubo's calculations for a small, almost spherical, metallic particle[42]:

$$\delta = 4m_e\nu_F^2/3n\pi L^3 \tag{2}$$

where m_e is the free electron mass, $\nu_F = 10^6$ ms^{-1} is a typical Fermi velocity for graphene, and $n = 2.3$ g cm^{-3} is the atomic density of the carbon nanospheres. These values yield an effective linear particle size of $L = 40$ nm. This particle size is in good agreement with that obtained from TEM images. Furthermore, the increase in T_1 and T_2 as the temperature is decreased (Fig. 4a and see also Supplementary Fig. 12) is characteristic to metals[21,41,45], where electron–phonon scattering due to spin–orbit interaction is responsible for the temperature-induced shortening of T_1 and T_2 (refs 42,45,46).

As the temperature was decreased, T_2 reached 300 ns at 4 K while T_1 reached 450 ns (Fig. 4a). There is a deviation from the $T_1 = T_2$ dependence below ∼100 K. During the delineation of T_1 and T_2 below ∼100 K, T_1 and T_2 nevertheless continue to increase at different rates. The electron spin dynamics of T_1 is
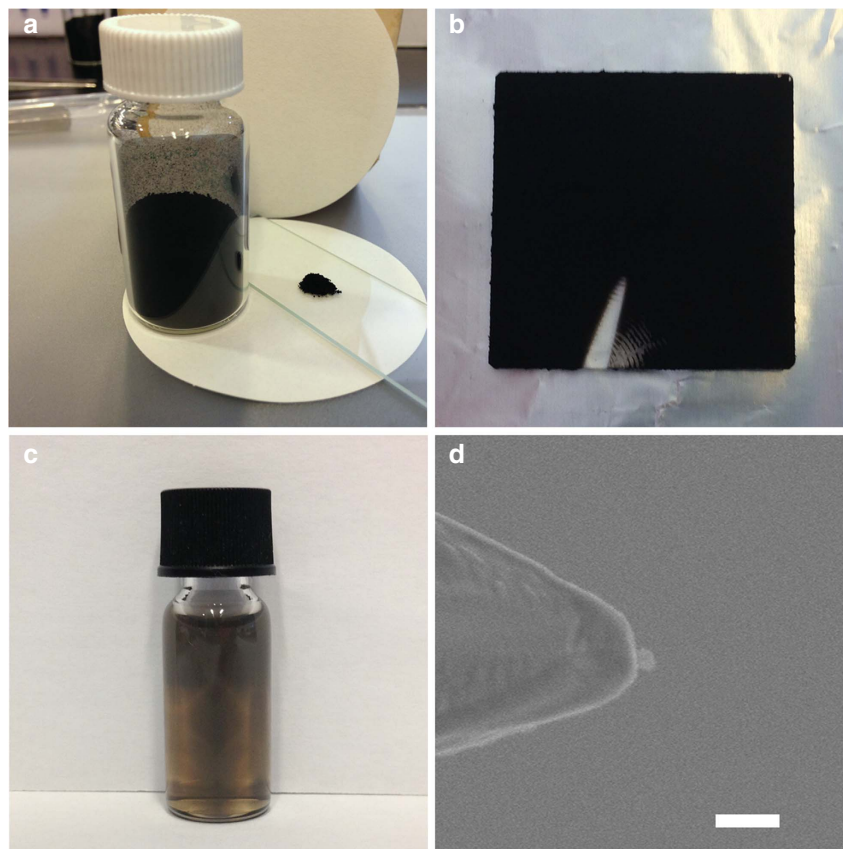
Figure 3 | Sample processing of carbon nanospheres. (**a**) A 300 mg of carbon nanospheres collected as a solid powder in a sample tube and 10 mg on a glass slide, stable in air. (**b**) Carbon nanospheres directly deposited during synthesis onto a 2.5×2.5 cm quartz slide. (**c**) A small amount of carbon nanospheres dispersed in 2 ml of ethanol by sonication. (**d**) SEM image of an individual ~ 50 nm carbon nanosphere physically positioned on a Si substrate using a 200-nm tungsten manipulator tip. Scale bar, 200 nm (**d**).

directly related to phonon dampening in disordered graphitic sheets[27,41] and the existence of Wallis-type[47] local phonon modes. Future studies have to show if further localization at specific defect sites occurs at very low temperatures. As the temperature is increased, the calculations of Andersson *et al.*[41] indicate that the observed shortening of T_1 and T_2 is caused by the scattering of conduction electrons by the potentials of peripheral atoms having edge-inherited electronic and lattice dynamical features and the excitation of low-energy phonons.

From our structural, chemical and electronic characterization we propose that the non-bonding orbitals associated to the structural imperfections induce conduction electrons to the system and significantly enhance the electron density of states. This is in agreement with theoretical works[41,48] that predict the presence of an additional band superimposed upon the bonding π and the anti-bonding $\pi^\star$ bands around the Fermi energy in nanometre size disordered graphitic fragments, and our observations of the changes in the p_z wave functions in the $p-\pi$ band evolutions with temperature near the Fermi energy level (Supplementary Fig. 5).

The carbon nanospheres also contain covalently bonded oxygen that contributes to the disorder within the graphitic lattices (Fig. 3f–h; Supplementary Table 1; Supplementary Fig. 9). We note that the removal of oxygen groups by thermal decomposition introduces non-bonding π and σ orbitals (Supplementary Figs 4 and 5). In future experiments, greater robustness against spin decoherence may be achieved by the removal of adatoms to enhance the electronic density of states[33].

Although the carbon nanospheres are highly defective, the intrinsically weak spin−orbit interaction of carbon has allowed for long T_1 and T_2 to persist even at 300 K. In nanotubes and fullerenes, an increase in spin−orbit coupling due to graphene sheet curvature may contribute to the shortening of T_1 and T_2 (refs 28,29), however the individual graphitic flakes in the carbon nanospheres are not curved. The $T_1 = T_2$ in the carbon nanospheres is remarkably a two orders of magnitude enhancement over that found in conducting crystalline graphene[32]. We attribute part of this increase in T_1 and T_2 to quantum confinement effects readily observed in conducting nanostructures[9,11,12,21].

Following our observations of magnetically induced spin polarization, we coherently rotated the electron spin at 300 K by applying microwave power bursts of increasing duration and with variable power (Fig. 5a). We observed that the magnetization of the carbon nanospheres oscillates periodically with pulse duration, the oscillation frequency being proportional to the square root of the microwave power. This oscillation indicates that we have performed deliberate and coherent electron spin rotations (driving of electron spins between two Zeeman-split energy levels), or Rabi oscillations. This is the sign that one can manipulate spins both for spintronics and quantum information processing (see also Supplementary Note 4)[1,49]. Fourier-transformed Rabi oscillation signals show a single-component characteristic to electron spin-1/2 qubit (Fig. 5b). A key characteristic of the Rabi process is a linear dependence of the Rabi frequency on the microwave field strength $\mathbf{B}_1$ ($f_{Rabi} = g\mu_B\mathbf{B}_1/h$). We verify this by extracting the Rabi frequency from a fit of the
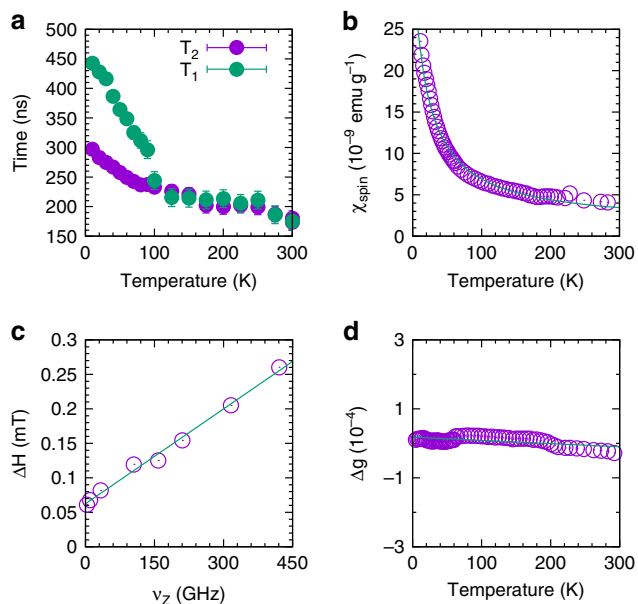
Figure 4 | Characterization of the spin system of the carbon spheres by ESR. (**a**) Temperature dependence of T_1 and T_2 at $v_Z = 9.5$ GHz. (**b**) Temperature dependence of the spin susceptibility, χ_{spin}, measured by ESR at $v_Z = 9.4$ GHz with an overlaying Curie − Weiss line, characteristic to small paramagnetic particles. (**c**) The ESR linewidth is plotted as a function of the Zeeman energy, $E_Z = hv_Z$ measured by a multi-frequency ESR at 300 K. The linear fit (straight solid line) using equation (1), with $T_1 = T_2 = 175$ ns gives $\delta = 1$ meV. (**d**) The temperature-independent g-factor shift Δg relative to the free electron g-value, in good agreement with a material exhibiting very weak spin − orbit coupling. Error bars represent the confidence interval of least square fits to the spectra.

Fourier-transformed signal of Fig. 5b with a Gaussian line, which gives the expected linear behaviour that is proportional to $\mathbf{B}_1$ (Fig. 5c). This demonstrated the capacity to rotate the spin qubits on the carbon nanospheres arbitrarily to any point on the Bloch sphere[3] at temperatures as high as 300 K. Rabi oscillations can be observed for ∼400 ns, consistent with decoherence by T_2. The increase in linewidth of the Fourier-transformed oscillations with microwave power (Fig. 5b) is caused by microwave field inhomogeneity.

Discussion

We have demonstrated that a long itinerant electron spin lifetime in a magnetically homogenous conducting material can be achieved at room temperature. Through the controlled polarization of coherent electron spins in these carbon nanospheres, we have showed that this electron spin lifetime exceeds the prerequisite for applications in spintronics and quantum information processing. This is possible through electron confinement to nanometre-sized, non-crystalline yet metallic-like carbon spheres. This work effectively bridges the disparate research directions in the fields of inorganic and molecular materials for electron spin qubits and has broad applicability: spin qubits can now be manipulated at room temperature without the need for isotopically engineering a host material, diluting the spin-carrying molecule, cryogenic temperatures, the preparation of well-defined crystal structures, or the use of metals. The facile preparation of a carbon material using common laboratory reagents, combined with the use of well-established electron spin manipulation measurements at room temperature, effectively reduces many of the technological barriers to realising practical quantum computing and spintronics using solid-state materials.
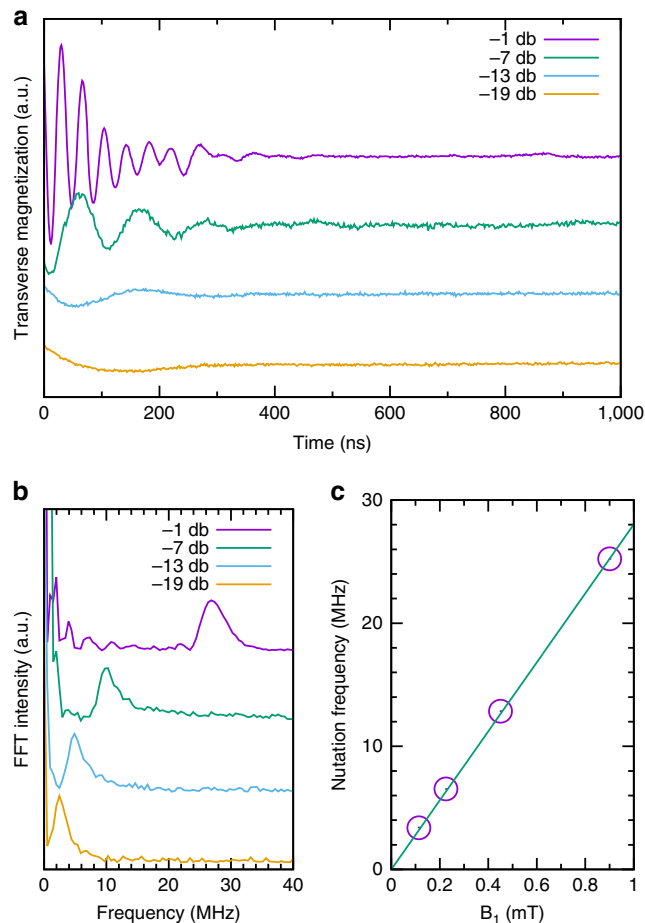

Figure 5 | Spin control over electron qubits confined to carbon nanospheres at 300 K. (**a**) Rabi oscillations of the electron qubits at 300 K and $B_0 = 337$ mT for different microwave powers. (**b**) Fourier transform of the Rabi oscillations, with the signal shifted vertically for clarity. (**c**) Rabi frequency is proportional with the square root of the power. The value 25 MHz observed for the maximum power is consistent with the previously determined maximum B_1 field in the dielectric cavity of 0.9 mT, indicating the presence of an effective spin $S = 1/2$.

The spin-manipulation experiments described here were performed on a large number of carbon nanospheres. Although the material can be readily chemically processed, it is prepared in a form suitable for device processing: we have demonstrated that the conducting nanospheres can be isolated on a silicon surface by physically manipulating individual nanospheres. In principal, this may provide an initial avenue to high-density qubit arrays of nanospheres that are integrated onto existing silicon technologies or thin-film-based electronics.

Methods

recorder software v2.48.1.1 was used to collect the topography images. JEOL Composer and JEOL Visualizer-kai programs were used to reconstruct the tomography images.

Scanning electron microscopy. Scanning electron microscopy was performed using a Zeiss Ultra Plus.

X-ray photoelectron spectroscopy. Measurements were conducted using an ESCALAB250Xi instrument manufactured by Thermo Scientific, UK. The background vacuum was better than 2×10^{-9} mbar. A monochromated Al K_α (energy $hv = 1,486.68$ eV) was used with a spot size of 500 µm. The fine carbon powder was manually pressed onto indium foil for analysis or pressed into a disc prior to *in situ* heating experiments. Curve fitting was performed using the Scienta ESCA300 data-system software. Binding energy reference was C $1s = 285.0$ eV for adventitious carbon.

Raman spectroscopy. Raman spectroscopy was performed using Argon 514 nm excitation laser on a Renishaw Raman inVia Reflex with a notch and edge filter cutoff of 100 cm^{-1}.

Modulated thermogravimetric analysis. Modulated thermogravimetric analysis measurements were obtained using a TA HiRes Discovery TGA in modulated TGA mode with a heating profile of 2 °C min^{-1} under the flow of 20 ml min^{-1} high-purity N$_2$ with sinusoidal temperature amplitude of 4 °C and period of 200 s. A 100-µl alumina pan was used. Evolved gas analysis (TGA GC–MS) was performed using a Perkin Elmer Thermogravimetric Analyzer Pyris 1 coupled to a Perkin Elmer Gas Chromatograph Clarus 680 and Mass Spectrometer Clarus SQ 8 C.

Continuous-wave ESR. Experiments were performed on a home built quasi-optical spectrometer operated in the 55–420 GHz frequency range in a corresponding 0–16 T field range[43,44]. At low frequencies of 4, 9.4 and 34 GHz, a Bruker elexsys E500 spectrometer was used. For a typical experiment, about 1 mg of the carbon sample was weighed and then sealed in a quartz ESR tube after being heated at 500 K under dynamic vacuum overnight. For temperature- and frequency-dependent experiments, the magnetic field modulation amplitude was smaller than 0.01 mT and the microwave power was set to 0.2 µW to avoid signal distortion. For *g*-factor reference, a polycrystalline KC$_{60}$ powder was used with $g = 2.0006$.

Pulsed ESR. Experiments were performed at 9.4 and 34 GHz using Bruker ElexSys 580 and 680 spectrometers. For T_2 determination we used a simple 2-pulse sequence, invoking a first $\pi/2$ pulse of 16 ns, and an initial delay of the second pulse of 300 ns. The resulting echo was integrated over 175 ns. For T_1, a 3-pulse sequence was used. An initial π pulse of 32 ns was followed after 300 ns delay by a 2-pulse echo sequence with 200 ns initial pulse delay for monitoring the inversion recovery. For Rabi experiments, a single $\pi/2$ pulse was used. Its length was incremented by 2 or 4 ns. After a delay of ~ 84 ns with respect to the pulse ending, the signal was observed with a short integrating time of 16 ns.

Data availability. The data that support the findings of this study are available from the corresponding authors upon request.

References

1. DiVincenzo, D. P. Quantum computation. *Science* **270,** 255 (1995).
2. Poole, C. P. J & Farach, H. A. *Relaxation in Magnetic Resonance* (Academic Press, 1971).
3. Bloch, F. Nuclear induction. *Phys. Rev.* **70,** 460 (1946).
4. Jánossy, A. Resonant and nonresonant conduction-electron-spin transmission in normal metals. *Phys. Rev. B* **21,** 3793–3810 (1980).
5. Ardavan, A. *et al.* Will spin-relaxation times in molecular magnets permit quantum information processing? *Phys. Rev. Lett.* **98,** 057201 (2007).
6. Awschalom, D. D. & Flatte, M. E. Challenges for semiconductor spintronics. *Nat. Phys.* **3,** 153–159 (2007).
7. Zwanenburg, F. *et al.* Silicon quantum electronics. *Rev. Mod. Phys.* **85,** 961–1019 (2013).
8. Wolf, S. A. *et al.* Spintronics: a spin-based electronics vision for the future. *Science* **294,** 1488–1495 (2001).
9. Yang, C. H. *et al.* Spin-valley lifetimes in a silicon quantum dot with tunable valley splitting. *Nat. Commun.* **4,** 2069 (2013).
10. Dzhioev, R. *et al.* Low-temperature spin relaxation in n-type GaAs. *Phys. Rev. B* **66,** 245204 (2002).
11. Yakushiji, K. *et al.* Enhanced spin accumulation and novel magnetotransport in nanoparticles. *Nat. Mater.* **4,** 57–61 (2005).
12. Hai, P. N., Ohya, S. & Tanaka, M. Long spin-relaxation time in a single metal nanoparticle. *Nat. Nanotechnol.* **5,** 593–596 (2010).
13. Colless, J. I. *et al.* Dispersive readout of a few-electron double quantum dot with fast rf gate sensors. *Phys. Rev. Lett.* **110,** 046805 (2013).
14. Morton, J. J. L. *et al.* Bang-bang control of fullerene qubits using ultrafast phase gates. *Nat. Phys.* **2,** 40–43 (2006).
15. Loss, D. & DiVincenzo, D. P. Quantum computation with quantum dots. *Phys. Rev. A.* **57,** 120 (1998).
16. Awschalom, D. D., Bassett, L. C., Dzurak, A. S., Hu, E. L. & Petta, J. R. Quantum spintronics: engineering and manipulating atom-like spins in semiconductors. *Science* **339,** 1174–1179 (2013).
17. Warner, M. *et al.* Potential for spin-based information processing in a thin-film molecular semiconductor. *Nature* **503,** 504–508 (2013).
18. Aromi, G., Aguila, D., Gamez, P., Luis, F. & Roubeau, O. Design of magnetic coordination complexes for quantum computing. *Chem. Soc. Rev.* **41,** 537–546 (2012).
19. Chuang, P. *et al.* All-electric all-semiconductor spin field-effect transistors. *Nat. Nanotechnol.* **10,** 35–39 (2015).
20. Feher, G. & Kip, A. Electron spin resonance absorption in metals. I. Experimental. *Phys. Rev.* **98,** 337 (1955).
21. Halperin, W. P. Quantum size effects in metal particles. *Rev. Mod. Phys.* **58,** 533–606 (1986).
22. Boross, P., Dóra, B., Kiss, A. & Simon, F. A unified theory of spin-relaxation due to spin-orbit coupling in metals and semiconductors. *Sci. Rep.* **3,** 3233 (2013).
23. Zhou, Y. *et al.* Electrical spin injection and transport in germanium. *Phys. Rev. B* **84,** 125323 (2011).
24. Toshio, S. *et al.* Room-temperature electron spin transport in a highly doped Si channel. *Appl. Phys. Exprqess* **4,** 023003 (2011).
25. Childress, L. *et al.* Coherent dynamics of coupled electron and nuclear spin qubits in diamond. *Science* **314,** 281–285 (2006).
26. Weiden, N., Käss, H. & Dinse, K. P. Pulse electron paramagnetic resonance (EPR) and electron − nuclear double resonance (ENDOR) investigation of N@C60 in polycrystalline C60. *J. Phys. Chem. B.* **103,** 9826–9830 (1999).
27. Náfrádi, B., Choucair, M. & Forró, L. Spin lifetime of itinerant electrons in chemically synthesized graphene multi-layers. *Carbon NY* **74,** 346–351 (2014).
28. Churchill, H. O. H. *et al.* Relaxation and dephasing in a two-electron ^{13}C nanotube double quantum dot. *Phys. Rev. Lett.* **102,** 166802 (2009).
29. Huertas-Hernando, D., Guinea, F. & Brataas, A. Spin-orbit coupling in curved graphene, fullerenes, nanotubes, and nanotube caps. *Phys. Rev. B* **74,** 155426 (2006).
30. Novoselov, K. S. *et al.* Electric field effect in atomically thin carbon films. *Science* **306,** 666–669 (2004).
31. Meyer, J. C. *et al.* The structure of suspended graphene sheets. *Nature* **446,** 60–63 (2007).
32. Drögeler, M. *et al.* Nanosecond spin lifetimes in single- and few-layer graphene–hBN heterostructures at room temperature. *Nano. Lett.* **14,** 6050–6055 (2014).
33. Náfrádi, B., Choucair, M., Southon, P. D., Kepert, C. J. & Forró, L. Strong interplay between the electron spin lifetime in chemically synthesized graphene multilayers and surface-bound oxygen. *Chemistry* **21,** 770–777 (2015).
34. Moro, F. *et al.* Coherent electron spin manipulation in a dilute oriented ensemble of molecular nanomagnets: pulsed EPR on doped single crystals. *Chem. Commun.* **50,** 91–93 (2014).
35. Moro, F., Turyanska, L., Granwehr, J. & Patanè, A. Spin manipulation and spin-lattice interaction in magnetic colloidal quantum dots. *Phys. Rev. B* **90,** 205428 (2014).
36. Choucair, M. & Stride, J. A. The gram-scale synthesis of carbon onions. *Carbon NY* **50,** 1109–1115 (2012).
37. Kahlert, J. U. *et al.* Site-specific synthesis of a hybrid boron-graphene salt. *Chem. Commun.* **52,** 1290–1292 (2016).
38. Kahlert, J. U., Rawal, A., Hook, J. M., Rendina, L. M. & Choucair, M. Carborane functionalization of the aromatic network in chemically-synthesized graphene. *Chem. Commun.* **50,** 11332–11334 (2014).
39. Harneit, W. Fullerene-based electron-spin quantum computer. *Phys. Rev. A.* **65,** 032322 (2002).
40. Shames, A. I. *et al.* Defects and impurities in nanodiamonds: EPR, NMR and TEM study. *J. Phys. Chem. Solids* **63,** 1993–2001 (2002).
41. Andersson, O. *et al.* Structure and electronic properties of graphite nanoparticles. *Phys. Rev. B* **58,** 16387–16395 (1998).
42. Kubo, R. Electronic properties of metallic fine particles. I. *J. Phys. Soc. Jpn* **17,** 975–986 (1962).
43. Náfrádi, B., Gaál, R., Fehér, T. & Forró, L. Microwave frequency modulation in continuous-wave far-infrared ESR utilizing a quasi-optical reflection bridge. *J. Magn. Reson.* **192,** 265–268 (2008).
44. Náfrádi, B., Gaál, R., Sienkiewicz, A., Fehér, T. & Forró, L. Continuous-wave far-infrared ESR spectrometer for high-pressure measurements. *J. Magn. Reson.* **195,** 206–210 (2008).
45. Elliott, R. J. Theory of the effect of spin-orbit coupling on magnetic resonance in some semiconductors. *Phys. Rev.* **96,** 266–279 (1954).
46. Kawabata, A. Electronic properties of fine metallic particles. III. E.S.R. absorption line shape. *J. Phys. Soc. Jpn* **29,** 902–911 (1970).

47. Wallis, R. F. Theory of surface modes of vibration in two- and three-dimensional crystal lattices. *Phys. Rev.* **116,** 302–308 (1959).
48. Yazyev, O. V. & Louie, S. G. Electronic transport in polycrystalline graphene. *Nat. Mater.* **9,** 806–809 (2010).
49. Bellac, M. L. *A Short Introduction to Quantum Information and Quantum Computation* (Cambridge University Press, 2006).
50. Morton, J. J. L. *et al.* Solid-state quantum memory using the 31P nuclear spin. *Nature* **455,** 1085–1088 (2008).

Acknowledgements

Author contributions

M.C. synthesized the materials. M.C., B.N. and K.-P.D. derived the experimental results. All authors discussed the results and contributed to the writing of the manuscript.

Additional information

Supplementary Information accompanies this paper at http://www.nature.com/naturecommunications.

Competing financial interests: The authors declare no competing financial interests.

Reprints and permission information is available online at http://npg.nature.com/reprintsandpermissions/

How to cite this article: Náfrádi, B. *et al.* Room temperature manipulation of long lifetime spins in metallic-like carbon nanospheres. *Nat. Commun.* **7:**12232 doi: 10.1038/ncomms12232 (2016).